

# Optimizing Serially Concatenated Neural Codes with Classical Decoders

Jannis Clausius, Marvin Geiselhart and Stephan ten Brink

Institute of Telecommunications, University of Stuttgart, Pfaffenwaldring 47, 70659 Stuttgart, Germany

{clausius,geiselhart,tenbrink}@inue.uni-stuttgart.de

**Abstract**—For improving short-length codes, we demonstrate that classic decoders can also be used with real-valued, neural encoders, i.e., deep-learning based “codeword” sequence generators. Here, the classical decoder can be a valuable tool to gain insights into these neural codes and shed light on weaknesses. Specifically, the turbo-autoencoder is a recently developed channel coding scheme where both encoder and decoder are replaced by neural networks. We first show that the limited receptive field of convolutional neural network (CNN)-based codes enables the application of the BCJR algorithm to optimally decode them with feasible computational complexity. These maximum a posteriori (MAP) component decoders then are used to form classical (iterative) turbo decoders for parallel or serially concatenated CNN encoders, offering a close-to-maximum likelihood (ML) decoding of the learned codes. To the best of our knowledge, this is the first time that a classical decoding algorithm is applied to a non-trivial, real-valued neural code. Furthermore, as the BCJR algorithm is fully differentiable, it is possible to train, or fine-tune, the neural encoder in an end-to-end fashion.

## I. INTRODUCTION

The channel coding problem for long block lengths has been essentially solved: Over the past decades, powerful and efficient coding schemes such as turbo codes [1] and low-density parity-check (LDPC) codes [2] have been developed which perform near the Shannon capacity of the additive white Gaussian noise (AWGN) channel. However, good encoder-decoder pairs for short block lengths (i.e., in the order of a hundred bits) which are required for ultra-reliable low-latency communication (URLLC) scenarios are yet to be found.

Meanwhile, deep learning based methods made their way into communication systems and channel coding in particular. Early works [3] [4] demonstrated that general neural networks (NNs) are able to learn the decoding of classically (i.e., polar and convolutionally) coded sequences. Models working on the Tanner graph of a code were shown to even outperform classical decoding algorithms for short codes [5] [6].

Soon, the question arose whether also the encoder (i.e., the code itself) can be learned as a NN. The use of an autoencoder to jointly optimize encoder and decoder was proposed in [7]. The main difference to previous methods is that the autoencoder is trained end-to-end in an unsupervised fashion.

However, naïve implementations of autoencoders do not scale to practical block lengths and, thus, do not exhibit

This work is supported by the German Federal Ministry of Education and Research (BMBF) within the project Open6GHub under grant 16KISK019 and the project FunKI under grant 16KIS1187.

TABLE I: Selected related work on classical and deep-learning based channel coding schemes

	Classical Decoding	Deep Learning based Decoding
Classical Encoding	Turbo codes [1] LDPC codes [2]	Dense Neural Networks [3] RNN-based conv. decoding [4] Weighted belief propagation [5] Graph Neural Networks [6]
Deep Learning based Encoding	<b>This work</b>	Autoencoder [7] Turbo Autoencoder [8] K.O. codes [12]

competitive coding gains. The authors of [8] propose the turbo-autoencoder to solve these issues. The main idea is to use two or more concatenated convolutional neural network (CNN)-based encoder networks together with iterative decoding networks — the same principle as used in turbo codes. Recent research improved the turbo-autoencoder by also optimizing the interleaver permutation [9] and sped up training using Gaussian pre-training [10]. Moreover, [11] demonstrated that the serial turbo-autoencoder can be extended to also perform joint detection, synchronization and equalization, outperforming state-of-the-art classical schemes. Another related concept of learning encoder and decoder, using the archetype of polar codes (rather than turbo codes), was proposed in [12].

Table I arranges these prior works in two dimensions: Whether classical (i.e., engineered) or deep-learning based models are used for the encoder and decoder, respectively. The evolution outlined above moved from classical systems to first making the decoder trainable, and then learning the encoder as well. A natural question to ask is whether it is also possible to use classical decoders with neural encoders. As classical decoders are better understood, this can serve as a valuable tool to analyze and fine-tune neural codes. The main contributions of this paper are as follows:

- We derive a low-complexity method for analyzing the effective memory learned by the CNN-based encoders and show that it is much shorter than what their receptive field potentially would allow.
- We present how the Bahl-Cocke-Jelinek-Raviv (BCJR) algorithm can be applied to decode learned CNN codes with quasi-maximum a posteriori (MAP) performance. The BCJR-based turbo decoder is then applied to decode trained serially concatenated neural codes (SCNCs).
- We show that using the BCJR-based decoder, neural encoders can be fine-tuned or even trained from scratch to obtain improved performance.

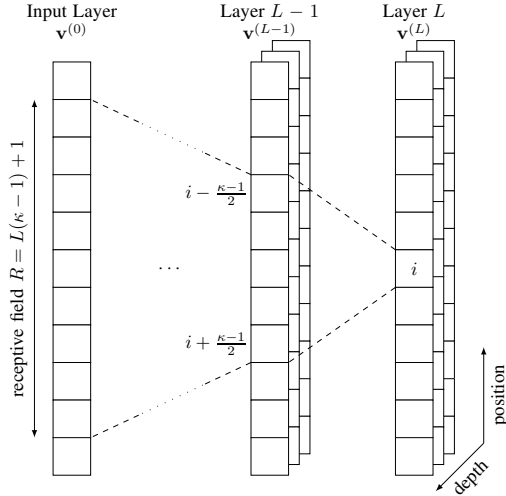


Fig. 1: Visualization of the receptive field of a CNN with kernel size  $\kappa = 5$ . The positional axis is arranged vertically, the different feature maps are indicated in the depth dimension.

## II. PRELIMINARIES

### A. Convolutional Neural Networks

A commonly used class of feed-forward neural networks are CNNs. Each layer can be mathematically described by a convolution operation of the input and trainable filter kernels, followed by a non-linear activation function. The CNNs used in the turbo autoencoder use one-dimensional (1D) convolutions over the *positional* axis. Each layer can have a depth of multiple such one-dimensional *feature maps* and has independent trainable filter kernels of size  $\kappa$  for each combination of input and output feature maps. As illustrated in Fig. 1, the output of any layer only depends on  $\kappa$  elements of the previous layer. Hence, after  $L$  convolutional layers with kernel size  $\kappa$ , the number of input symbols affecting each output symbol is limited to  $R = L \cdot (\kappa - 1) + 1$ . This number is called the *receptive field* of the CNN.

### B. Serial Turbo Autoencoder based System

General-purpose dense neural networks (DNNs) or CNNs are not able to learn codes that are comparable to state-of-the-art (binary) channel codes due to the *curse of dimensionality* [8], [13]. To overcome this problem and learn competitive, neural channel codes for messages  $\mathbf{u}$  longer than  $k > 16$  bits, the serial turbo-autoencoder [8], [10] has been proposed. The serial turbo-autoencoder is an autoencoder that employs the structure of serially concatenated codes with an iterative decoder. The architecture is displayed in Fig. 2 for the encoder and in Fig. 3 for the decoder. While the overall structure of this end-to-end trainable system is carefully chosen, the constituent components are general-purpose CNNs. In addition to the proposed turbo-autoencoders in [8], [10], we employ the advancements of circular convolutions from [14], [13] and the linear interleaver from [14]. Note, that the circular padding in the encoder can be interpreted as tail-biting encoding.

Fig. 2 shows the encoder of the serial turbo-autoencoder. It consists of a cascade of an outer encoder  $f_O(\cdot)$ , an interleaver

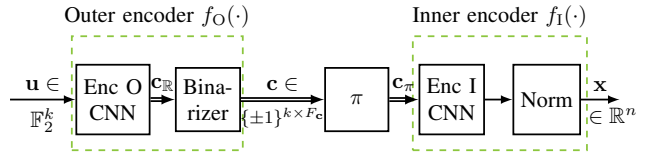


Fig. 2: Serially concatenated CNN-based encoder structure of the transmitter learning a real-valued serially concatenated neural code (SCNC).

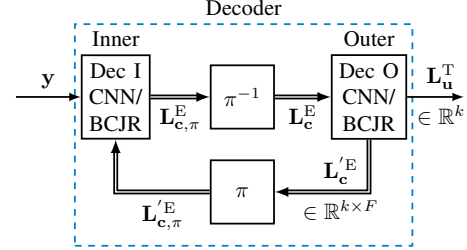


Fig. 3: Serial CNN- or BCJR-based turbo decoder structure.

and an inner encoder  $f_I(\cdot)$ . The hyperparameters that are used for all CNNs are shown in Tab. II. The CNN of the outer encoder sees the uncoded message  $\mathbf{u} \in \{-1, 1\}^k$  and encodes it into a real-valued sequence  $\mathbf{c}_R^{k \times F_c}$ , where  $F_c$  is a hyperparameter denoting the depth of the outputs (illustrated by double arrows in Fig. 2). Subsequently, the real-valued, coded sequence  $\mathbf{c}_R$  is binarized, so  $\mathbf{c} = \text{sign}(\mathbf{c}_R)$ . Note, as the derivative  $\frac{\partial \text{sign}(x)}{\partial x} = 0$  almost everywhere, we replace the derivative for back-propagation with a linear function with saturation effects

$$\frac{\partial \text{sign}(x)}{\partial x} = \begin{cases} 1 & \text{for } |x| < 1 \\ 0 & \text{else.} \end{cases} \quad (1)$$

This is known as the saturated straight-through estimator (STE) [15]. In a next step, the coded sequence  $\mathbf{c}$  with  $k$  *positional* entries and  $F_c$  *depth* entries is interleaved over the positional dimension. Finally, the inner encoder (Enc I) computes the  $n$  symbols  $\mathbf{x}^{k \times F_x}$  which then are normalized and transmitted. Note, that the rate of the SCNC is  $r = k/n = 1/F_x$ .

The iterative structure for decoding serially concatenated codes is shown in Fig. 3. The inner decoder (Dec I) sees the channel observations  $\mathbf{y} \in \mathbb{R}^{k \times F_x}$  and the a priori information from the outer decoder (Dec O). In the first iteration the a priori information is initialized as  $\mathbf{L}_{c,\pi}^E = \mathbf{0}$ , where the subscript, i.e.,  $c$ , denotes the bits which the information is about. Then the extrinsic information of the inner decoder is interleaved and forwarded to the outer decoder. The outer decoder outputs an estimate  $\mathbf{L}_u^T$  of the uncoded bits  $\mathbf{u}$  and the extrinsic information  $\mathbf{L}_c^E$ , which is the a priori information for the inner decoder.

The serial turbo-autoencoder can be trained in an end-to-end fashion as all components are differentiable. We employ the same training methods as in [8]. The hyperparameters for the training are shown in Tab. II. Note, we use a random interleaver for training and a linear interleaver during inference. As loss function we chose the binary cross-entropy (BCE) function. It is worth mentioning that the learning schedule for

TABLE II: Hyperparameters for architecture and training the serial turbo-autoencoder

Parameter	Value	Parameter	Value
CNN filters	100	Loss	BCE
CNN kernel	5	$T_{\text{TX}}$	100
Layers per CNN	5	$T_{\text{RX}}$	500
Receiver iters.	6	Batch size	500 – 4000
$F_c$	10	Optimizer	ADAM
$(k, n)$	(64, 128)	Learning rate	$10^{-4} – 10^{-6}$
Train. interleaver	random	Encoder SNR	4.0 dB
Padding	Circular	Decoder SNR	0.5 – 4.0 dB

the encoder and decoder is alternating. That means, in a loop we calculate  $T_{\text{TX}}$  stochastic gradient descent (SGD) updates for the whole encoder while the decoder weights are fixed, and in a next step, we calculate  $T_{\text{RX}}$  SGD updates for the whole decoder while the encoder weights are fixed.

Similar to [10] and [11] we observe a significant amount of single-bit errors after decoding. This implies that the bit errors in the decoder are loosely correlated. As a result, the block error rate (BLER) can be drastically improved by an outer single-parity-check code and flipping the bit with the least reliability in case of a not matching parity. We consider the associated rate loss in form of a rate shift of  $10 \log_{10}(k-1/k)$  dB.

### C. Overview of the BCJR Algorithm

This subsection shortly introduces the log-domain BCJR algorithm [16] for decoding in a serial turbo decoder. The BCJR algorithm is an optimal decoder in the sense of the bit-wise MAP criterion. This decoding criterion is formulated by  $\arg \max_{u_i} p(u_i | \mathbf{y})$ , where the bit  $u_i$  is estimated based on the noisy sequence  $\mathbf{y}$ . The algorithm is based on the following equations:

$$\gamma_i(s', s) = \log(p(u_i)p(y_i|u_i)) \quad (2)$$

$$\alpha_i(s) = \max_{s'}^* [\alpha_{i-1}(s') + \gamma_i(s', s)] \quad (3)$$

$$\beta_{i-1}(s') = \max_s^* [\beta_{i-1}(s) + \gamma_i(s', s)] \quad (4)$$

$$\max^*(x, y) \triangleq \log(e^x + e^y) \approx \max(x, y) \quad (5)$$

Equation (2) is a branch metric that needs to be calculated for every transition  $(s', s)$  where  $u_i$  and  $y_i$  are the  $i$ th bit and observation, respectively, with  $i = 0, \dots, N - 1$ . The state transitions  $(s', s)$  are defined by the encoder. The recursive equations (3) and (4) are path metrics that traverse the trellis in a forward and a backward manner, respectively. Whether we use equation (5) or the given approximation coincides with the labeling *log-MAP* and *max-log* respectively. The performance loss due to the approximation is usually omittable, if a suitable damping factor is applied after every BCJR decoder. Once the branch and path metrics are calculated, a final soft decision can be made according to

$$L_{\mathbf{u},i} = \max_{U^1}^* [\alpha_{i-1}(s') + \gamma_i(s', s) + \beta_i(s)] - \max_{U^0}^* [\alpha_{i-1}(s') + \gamma_i(s', s) + \beta_i(s)] \quad (6)$$

where  $U^1$  and  $U^0$  are the sets that contain every transition that is associated with  $u_i = -1$  and  $u_i = 1$  respectively. Note

that the choice of  $U^1$  and  $U^0$  determines whether the output is regarding the coded or the uncoded bits.

In the case of serial turbo decoding as depicted in Fig. 3, the inner decoder sees the channel observation  $\mathbf{y}$  and the a priori information  $L_{\mathbf{c},i}^{\text{E}}$  of the outer decoder. Therefore, (2) is calculated as

$$\gamma_i(s', s) = \frac{1}{2} L_{\mathbf{c},i}^{\text{E}} \cdot c_{s',s} - \frac{|y_i - x_{s',s}|^2}{2\sigma^2} \quad (7)$$

where  $\sigma^2$  is the noise power. In contrast, the outer decoder only receives the a priori information from the inner decoder, and thus

$$\gamma_i(s', s) = \frac{1}{2} L_{\mathbf{c},i}^{\text{E}} \cdot c_{s',s}. \quad (8)$$

As all presented equations are differentiable we can calculate a gradient though the BCJR decoders and, therefore, also the (unrolled) turbo decoder. This enables the BCJR algorithm to be used in the turbo decoder structure not only for decoding, but also training in an end-to-end fashion.

A last comment needs to be made in this section regarding the tail-biting (circular padding) structure of the encoder. The structure determines that the state at the first position  $i = 0$  equals the state after the last position  $i = N$ . Thus, we need to set the initial path metrics  $\alpha$  and  $\beta$  accordingly. However, the initial state is unknown. One way to circumvent this problem is to consider the wrap-around trellis [17]. The initialization of the path metrics begins  $w$  positions before the first position at index  $i_{\text{start}} = -w \bmod N$  and  $i_{\text{end}} = N + w \bmod N$  for  $\alpha$  and  $\beta$ , respectively. In other words, the sequence  $\mathbf{y}' = [y_{-w \bmod N}, y_{-w+1 \bmod N}, \dots, y_{N+w \bmod N}]$  is decoded instead of  $\mathbf{y} = [y_0, y_1, \dots, y_{N-1}]$ .

## III. BCJR DECODING OF NEURAL CODES

In this section we derive how to decode a learned SCNC with a classical decoder, namely the BCJR decoder. Note that for this purpose, we assume that the serially concatenated neural code (SCNC) has been already trained in a turbo-autoencoder, as shown, e.g., in [10].

### A. Estimating the Effective Memory of the Neural Codes

This subsection shows how to estimate the effective memory of a CNN from the gradient and that the gradient is, indeed, a useful indicator. We define that the memory of the CNN consists of *those* input positions inside the receptive field of each output *that* significantly contribute to the output value. Whether decoding of CNN-based codes is feasible or not using the BCJR algorithm depends on the memory size of the CNNs which exponentially relates to the number of states in the trellis. As each BCJR decoder computes the likelihood of every possible symbol (inner decoder) or bit (outer decoder) of the respective encoder at every position, we need to pre-calculate the possible symbols and bits for the state transitions. The number of possible symbols for an encoder CNN is  $M = |\mathcal{F}|^m$ , where  $|\mathcal{F}|$  is the number of elements of the set of the input to the CNN and  $m$  is the effective size of the memory of the CNN. Note that the filters in the CNNs are not causal and, thus, the memory does not only include past inputs but

also future inputs. The memory of a CNN is upper bounded by the receptive field that is determined by the CNN structure. In this case the receptive field is  $R = 21$  which could result in up to  $M = |\mathbb{F}_2|^R \approx 2 \cdot 10^7$  symbols for the binary field  $\mathbb{F}_2$ . The usage of the binarizer ensures that all inputs to the CNNs in the encoder are binary.

As BCJR decoding with  $2^{R-1}$  states is not feasible, positions with low contribution to the output can be pruned. We propose an easy way to measure the contribution by calculating the average energy of the gradient

$$e_{\partial, \mathbf{v}}(j) = E \left[ \left| \frac{\partial f(\mathbf{v})}{\partial v_j} \right|^2 \right] \quad (9)$$

$$\approx \frac{1}{N_B} \sum_{i=0}^{N_B} \left| \frac{\partial f(\mathbf{v}_i)}{\partial v_{i,j}} \right|^2 \quad (10)$$

where  $\mathbf{v}_i$  is the  $i$ th input to the neural network  $f(\cdot)$  from a batch of size  $N_B$ . We interpret the expected gradient (change of the output by changing the input) as the exhibited error of omitting an input position. The gradient is usually a by-product of any deep learning framework, and therefore Eq. (9) is readily available. In our case it is sufficient to consider a single output, as the weight-sharing property of the CNN and the circular padding ensure that each output exhibits the same dependencies to its relative input positions. In a next step, we compare the energy of the gradients for each encoder to a threshold  $t$  to obtain the effective size  $m$  of the memory. If the energy is larger than the threshold, then we consider this position to contribute significantly to an output and, thus, is part of the memory. We denote the set of positions from the first to the last contributing position by  $\mathcal{J}$  with  $|\mathcal{J}| = m + 1$  and all positions outside  $\mathcal{J}$  by  $\bar{\mathcal{J}}$ .

Since the gradient only describes the behavior around the inputs  $\pm 1$ , we need to verify that a bit flip from  $\pm 1$  to  $\mp 1$ , respectively, exhibits a similar behavior. For this, we calculate the expected energy of the difference quotient per bit position for a bit flip as

$$e_{\Delta, \mathbf{v}}(j) = E \left[ \frac{|f(\mathbf{v}) - f(\mathbf{v} \odot (1 - 2\mathbf{e}_j))|^2}{\|2\mathbf{e}_j\|^2} \right] \quad (11)$$

$$= \frac{1}{4 \cdot 2^R} \sum_{\mathbf{v} \in \{\pm 1\}^R} |f(\mathbf{v}) - f(\mathbf{v} \odot (1 - 2\mathbf{e}_j))|^2 \quad (12)$$

where  $\mathbf{e}_j$  denotes the unit vector which is 1 exactly in position  $j$  and  $\odot$  denotes element-wise multiplication. Note, Eq. (11) corresponds to the actual expected error of omitting an input position. In the following analysis of the encoder CNNs we empirically verify that Eq. (9) is, indeed, an approximation of Eq. (11) up to a scaling factor.

### B. Outer Neural Encoder with Binary Output

The outer encoder implements the mapping  $f_O : \mathbb{F}_2^k \rightarrow \mathbb{F}_2^{k \times F_c}$ . This means in general the CNN can learn an encoding with a coding rate as low as  $1/F_c$ , here  $F_c = 10$ . We observed, however, that only two out of the  $F_c$  depth dimensions of the output vary dependent on the input, while the remaining

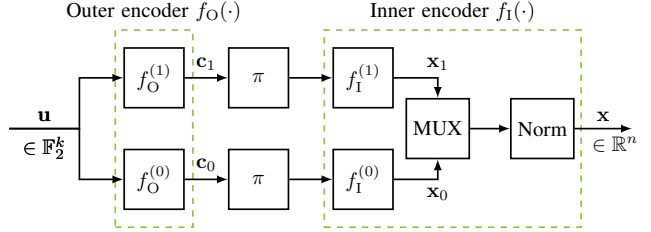


Fig. 4: Equivalent encoder block diagram. The outer encoder learns two output streams. Splitting the inputs to the inner encoder reduces the size of the memory  $m_{\mathbf{x}}^{(0)}$  and  $m_{\mathbf{x}}^{(1)}$ , respectively, to allow BCJR decoding at feasible complexity.

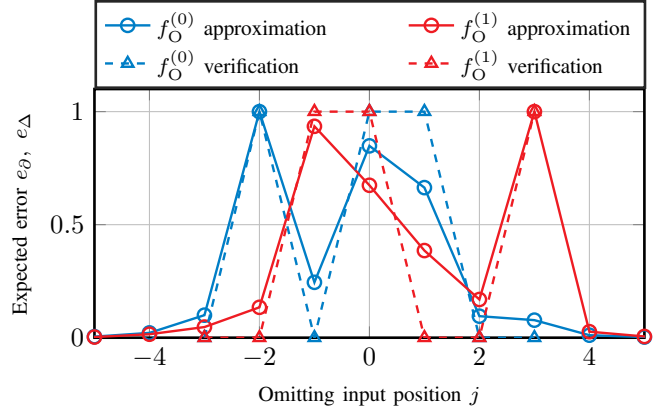


Fig. 5: Estimating the effective memory through the normalized expected error ( $e_{\partial}$  approximation,  $e_{\Delta}$  verification) of omitting input  $u_j$  in relation to each output for the outer encoders  $f_O(\cdot)$ .

eight depth dimensions stay fixed at either 1 or  $-1$  for all possible inputs. Therefore, a rate of  $1/2$  is learned which corresponds to the overall code rate of the concatenated neural encoders. We label the two dimensions with varying output  $\mathbf{c}^{(0)} = f_O^{(0)}(\mathbf{u})$  and  $\mathbf{c}^{(1)} = f_O^{(1)}(\mathbf{u})$ . This is illustrated in Fig. 4. It is remarkable to realize that the CNN learns this on its own without any injection of expert knowledge. Moreover, this observation aligns with the derivation from [18] that an outer code with a rate larger than the overall rate of a serial concatenated code is sub-optimal for iterative decoding.

Now we calculate Eq. (9) to estimate the memory and Eq. (11) for verification. The obtained plot for  $\mathbf{c}_0$  and  $\mathbf{c}_1$  is shown in Fig. 5. First of all, we want to mention that we expect a deviation of the approximation Eq. (9) as it does not capture the influence of the binarizer. Indeed, we observe a difference, albeit the general behavior matches. More interesting are the obtained values for  $e_{\Delta}$  which are either 1 or 0. This means that a bit flip in the respective input position either leads to a bit flip in all cases or in none. As a consequence, the outer encoder is equivalent to the linear generator polynomials  $G_0(Z) = Z^{-2} + Z^0 + Z^1$  and  $G_1(Z) = Z^{-1} + Z^0 + Z^3$ . This coincides with the reasoning from [16, p. 320] that the outer codes of serially concatenated turbo codes may be non-recursive and linear, while the inner codes have to be recursive or non-linear. The implication for decoding is that we can either run two BCJR decoders with memories  $m_c^{(0)} = 3$ ,  $m_c^{(1)} = 4$  and aggregate the bit estimates or run one BCJR decoder with memory  $m_c = 5$ . The first option can be

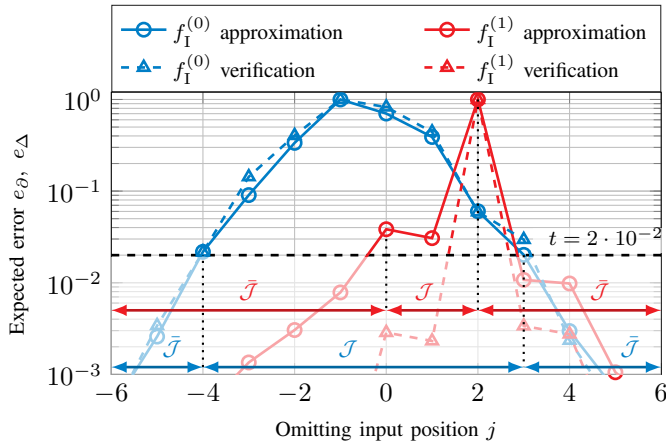


Fig. 6: Estimating the effective memory through the normalized expected error ( $e_\partial$  approximation,  $e_\Delta$  verification) of omitting input  $c_j$  in relation to each output for the inner encoders  $f_I(\cdot)$ . Positions with an error exceeding the threshold belong to the set of contributing positions  $\mathcal{J}$ .

chosen to save complexity. With this knowledge, we can precompute the output bits  $c_{s',s}$  for each of the  $2^{m_c+1} = 32$  state transitions  $(s',s)$ . Finally, we can plug  $c_{s',s}$  into the Eq. (8) and decode the outer neural code.

### C. Inner Neural Encoder with Real-valued Output

As we established in the last section that the coded bits  $\mathbf{c}$  have essentially dimensions  $k \times 2$ , the inner encoder learns the mapping  $\mathbb{F}_2^{k \times 2} \rightarrow \mathbb{R}^{k \times 2}$ . A problem is that the second depth dimension of the input roughly doubles the memory. To circumvent this problem, we first encode  $\mathbf{c}$  with  $\mathbf{c}^{(1)} = 1$  and then encode  $\mathbf{c}$  with  $\mathbf{c}^{(0)} = 1$ . This is illustrated in Fig. 4. Subsequently, we concatenate the first depth dimension of the first output with the second depth dimension of the second output to form output symbols  $\mathbf{x} = [\mathbf{x}^{(0)}, \mathbf{x}^{(1)}]$ . Effectively, the inner encoder consists of two functions  $\mathbf{x}^{(0)} = f_I^{(0)}(\mathbf{c}^{(0)})$  and  $\mathbf{x}^{(1)} = f_I^{(1)}(\mathbf{c}^{(1)})$ . Therefore, we show Eq. (9) and Eq. (11) for both encoding functions in Fig. 6. We observe that the approximation by the gradient closely follows the actual difference. Next we can set a threshold  $t$  to obtain the memory. We found that a threshold of  $t = 2 \cdot 10^{-2}$  does not degrade the final BLER. This leads to memory size  $m_x^{(0)} = 7$  for  $f_I^{(0)}(\cdot)$  and  $m_x^{(1)} = 2$  for  $f_I^{(1)}(\cdot)$ . However, the verification error  $e_\Delta$  of  $f_I^{(1)}$  indicates that actually an encoding without significant memory is learned. Thus, the learned encoding function  $f_I^{(1)}$  can be interpreted as a scaled binary phase shift keying (BPSK).

For the calculation of  $x_{s',s}$  in Eq. (7), we average  $x = f(\mathbf{c})$  with  $\mathbf{c} = [c_{-R/2}, \dots, c_{R/2}]$  over all possible values of  $c_j$  in positions  $j \in \mathcal{J}$  and  $c_j$  fixed for all  $j \in \mathcal{J}$ . Note that each transition  $(s',s)$  corresponds to exactly one value of the subvector  $\mathbf{c}_{\mathcal{J}}$  that contains  $c_j \forall j \in \mathcal{J}$ . This is done for both  $\mathbf{c}^{(0)}$  and  $\mathbf{c}^{(1)}$ .

## IV. RESULTS

### A. Decoding Performance

As performance metric we choose the BLER over the bit error rate (BER), as it is more relevant in systems with short

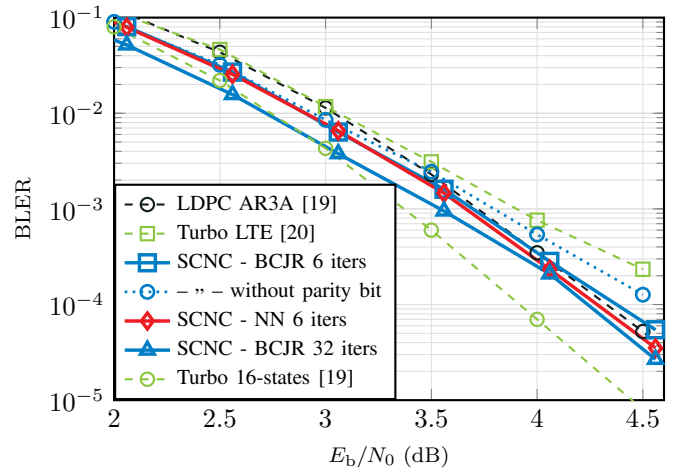


Fig. 7: Simulated BLER over an AWGN channel ( $k = 64$ ,  $n = 128$ ) for the serially concatenated neural code (SCNC) with a BCJR-based and a NN-based turbo decoder, respectively.

block lengths. In our transmission model we consider an AWGN channel. Further, we aim to transmit  $k = 64$  bits over  $n = 128$  channel uses, thus  $r = 0.5$ . The threshold for memory estimation is set to  $t = 2 \cdot 10^{-2}$  and we extend the wrap-around BCJR by  $w = 16$  positions in both directions. Fig. 7 shows the performance of the log-MAP BCJR-based turbo decoder for the SCNC with 6 iterations (—) and 32 iterations (—) respectively. Additionally, a curve without a parity bit and bit flip (···) is displayed, as described in section II-B. Recall that the number of states for the outer BCJR is set to  $2^{m_c} = 32$  and for the inner BCJR to  $2^{m_x^{(0)}} = 128$  and  $2^{m_x^{(1)}} = 2$ . For comparison, the same SCNC is shown with the matching CNN-based turbo decoder (—). Additionally, several baselines from [19] are shown and an additional LTE turbo code (—) [20] with 8 iterations of damped max-log decoding. We observe that the BCJR with 6 decoder iterations (—) shows slightly worse performance than the CNN decoder (—). However, 32 BCJR iterations (—) yield a significant gain for lower signal-to-noise-ratios (SNRs), but a negligible gain for higher SNRs. Thus, we conclude that the NN-based decoder operates close to its optimal performance for a high SNR. For the SCNC with a BCJR-based and NN-based decoder the LTE turbo code (—) is outperformed, however, there is a gap of 0.2 dB to the 16-states turbo code (—).

### B. Insights about the Turbo-Autoencoder

From the decoding of the SCNC with a classical decoder, we obtained insights regarding the turbo-autoencoder. To summarize the observations so far, Section III showed that the outer encoder learned a linear encoding and one of the inner encoder exhibits systematic behavior. The decoding results show that the learned NN-based decoder slightly outperforms the log-MAP BCJR-based decoder. Thus, the NN-based decoder displays close to optimal performance for the SCNC. This sets the spotlight on the encoder for potential improvements in performance. For both decoders we noticed a significant amount of single erroneous bits in a block error. For a SNR of

TABLE III: Hyperparameters for training and fine-tuning

Parameter	Value	Parameter	Value
Batch size	1000	Loss	BCE
Learning Rate	$10^{-5}$	Receiver iters.	2
SNR	4	SGD updates	1000

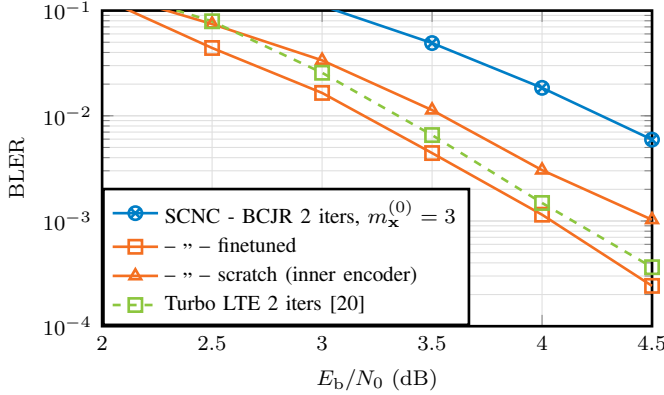


Fig. 8: Simulated BLER over an AWGN channel ( $k = 64$ ,  $n = 64$ ). Showcasing the training of serially concatenated neural code (SCNC) for a BCJR-based decoder with reduced memory  $m_x^{(0)} = 7 \rightarrow 3$  and reduced iterations  $6 \rightarrow 2$ .

4.5 dB the percentage of block errors with a single erroneous bit to all block errors is 71.5% and 66.0% for the BCJR-based and NN-based turbo decoder respectively. Conclusively, the minimal distance between code words seems to be small. Thus, the BLER is sub-optimal without an outer error-correcting code, which improves the minimum distance. A major factor for this behavior might be the BCE loss function, as it is known to minimize the BER and not the BLER [21].

### C. Training with BCJR decoders

As all equations for the BCJR-based turbo decoder are differentiable, we can train a neural encoder with a classical decoder. Here, we want to showcase this possibility for a reduction of the size of the memory  $m_x^{(0)} = 7 \rightarrow 3$  and the number of decoder iterations  $6 \rightarrow 2$ . The performance for this case for the not fine-tuned SCNC (— $\circ$ —) is displayed in Fig. 8. The fine-tuned SCNC with the same decoder (— $\square$ —) shows significant gain. Also it is possible to learn an encoder from scratch, i.e., the inner encoder (— $\triangle$ —). For reference, we plot the LTE turbo code with 2 iterations of damped max-log decoding (— $\square$ —). The hyperparameters for fine-tuning are listed in Tab. III. We found that a high batch size and a small learning rate are essential. Furthermore, the log-MAP BCJR lead to a smoother training with better performance than the max-log approximation.

## V. CONCLUSION

In this paper, we demonstrated that the BCJR decoding algorithm can be applied to CNN-based encoders. To mitigate computational complexity, we showed that only a fraction of the potentially learned memory in the encoder is required to decode the sequences, limiting the number of states in the decoder trellis. The resulting BCJR-based decoders can decode and fine-tune codes that have been learned as a turbo-autoencoder or even learn neural codes from scratch.

## REFERENCES

- C. Berrou, A. Glavieux, and P. Thitimajshima, “Near shannon limit error-correcting coding and decoding: Turbo-codes. 1,” in *Proceedings of ICC’93-IEEE International Conference on Communications*, vol. 2. IEEE, 1993, pp. 1064–1070.
- R. Gallager, “Low-density parity-check codes,” *IRE Transactions on Information Theory*, vol. 8, no. 1, pp. 21–28, 1962.
- T. Gruber, S. Cammerer, J. Hoydis, and S. ten Brink, “On deep learning-based channel decoding,” in *2017 51st Annual Conference on Information Sciences and Systems (CISS)*, 2017, pp. 1–6.
- D. Tandler, S. Dörner, S. Cammerer, and S. ten Brink, “On recurrent neural networks for sequence-based processing in communications,” in *2019 53rd Asilomar Conference on Signals, Systems, and Computers*, 2019, pp. 537–543.
- E. Nachmani, Y. Be’ery, and D. Burshtein, “Learning to decode linear codes using deep learning,” in *Allerton Conf. IEEE*, 2016, pp. 341–346.
- S. Cammerer, J. Hoydis, F. A. Aoudia, and A. Keller, “Graph neural networks for channel decoding,” in *IEEE Global Communications Conference (GLOBECOM) Workshop*, 2022.
- T. O’Shea and J. Hoydis, “An Introduction to Deep Learning for the Physical Layer,” *IEEE Trans. Cogn. Commun. Netw.*, vol. 3, no. 4, pp. 563–575, Dec. 2017.
- Y. Jiang, H. Kim, H. Asnani, S. Kannan, S. Oh, and P. Viswanath, “Turbo autoencoder: Deep learning based channel codes for point-to-point communication channels,” in *Advances in Neural Information Processing Systems*, vol. 32. Curran Associates, Inc., 2019.
- K. Chahine, Y. Jiang, P. Nuti, H. Kim, and J. Cho, “Turbo autoencoder with a trainable interleaver,” in *ICC 2022 - IEEE International Conference on Communications*, 2022, pp. 3886–3891.
- J. Clausius, S. Dörner, S. Cammerer, and S. ten Brink, “Serial vs. parallel Turbo-autoencoders and accelerated training for learned channel codes,” in *2021 11th International Symposium on Topics in Coding (ISTC)*, 2021.
- S. Dörner, J. Clausius, S. Cammerer, and S. ten Brink, “Learning joint detection, equalization and decoding for short-packet communications,” 2022. [Online]. Available: <https://arxiv.org/abs/2207.05699>
- A. V. Makkula, X. Liu, M. V. Jamali, H. Mahdavifar, S. Oh, and P. Viswanath, “Ko codes: inventing nonlinear encoding and decoding for reliable wireless communication via deep-learning,” in *Proceedings of the 38th International Conference on Machine Learning*, ser. Proceedings of Machine Learning Research, M. Meila and T. Zhang, Eds., vol. 139. PMLR, 18–24 Jul 2021, pp. 7368–7378. [Online]. Available: <https://proceedings.mlr.press/v139/makkula21a.html>
- H. Ye, L. Liang, and G. Y. Li, “Circular convolutional auto-encoder for channel coding,” in *2019 IEEE 20th International Workshop on Signal Processing Advances in Wireless Communications (SPAWC)*, 2019.
- H. Yildiz, H. Hatami, H. Saber, Y. Cheng, and J. H. Bae, “Interleaver design and pairwise codeword distance distribution enhancement for turbo autoencoder,” in *2021 IEEE Global Communications Conference (GLOBECOM)*, 2021, pp. 01–06.
- Y. Bengio, N. Léonard, and A. C. Courville, “Estimating or propagating gradients through stochastic neurons for conditional computation,” *arXiv:1308.3432*, 2013.
- W. E. Ryan and S. Lin, *Channel Codes: Classical and Modern*, 2009.
- J. Anderson and S. Hladik, “Tailbiting map decoders,” *IEEE Journal on Selected Areas in Communications*, vol. 16, no. 2, pp. 297–302, 1998.
- A. Ashikhmin, G. Kramer, and S. ten Brink, “Extrinsic information transfer functions: model and erasure channel properties,” *IEEE Transactions on Information Theory*, vol. 50, no. 11, pp. 2657–2673, 2004.
- G. Liva, L. Gaudio, T. Ninacs, and T. Jerkovits, “Code design for short blocks: A survey,” 10 2016.
- 3GPP, “Evolved Universal Terrestrial Radio Access (E-UTRA); Multiplexing and channel coding,” 3rd Generation Partnership Project (3GPP), Technical Specification (TS) 36.212.
- S. Cammerer, F. Ait Aoudia, S. Dörner, M. Stark, J. Hoydis, and S. ten Brink, “Trainable communication systems: Concepts and prototype,” *IEEE Transactions on Communications*, vol. 68, no. 9, pp. 5489–5503, 2020.